Electron capture and electron transport by fast ions penetrating solids: An open quantum system approach with sources and sinks

Marek Seliger,[1,2,*] Carlos O. Reinhold,[3,4] Tatsuya Minami,[3,5] David R. Schultz,[3] Michael S. Pindzola,[5] Shuhei Yoshida,[1] Joachim Burgdörfer,[1,4] Emily Lamour,[6] Jean-Pierre Rozet,[6] and Dominique Vernhet[6]

[1]*Institute for Theoretical Physics, Vienna University of Technology, A-1040 Vienna, Austria*

[2]*Institute for Physics, Karl-Franzens-University Graz, A-8010 Graz, Austria*

[3]*Physics Division, Oak Ridge National Laboratory, Oak Ridge, Tennessee 37831-6372, USA*

[4]*Department of Physics and Astronomy, University of Tennessee, Knoxville, Tennessee 37996-1200, USA*

[5]*Department of Physics, Auburn University, Auburn, Alabama 36849, USA*

[6]*Institut des NanoSciences de Paris, CNRS UMR 75-88, Universités Paris 6 et 7, 75015 Paris, France*

(Received 30 August 2006; published 19 March 2007)

We present a joint theoretical and experimental study of the time evolution of electronic states of highly charged hydrogenic ions formed by capture during transmission through solids as they undergo multiple collisions and radiative decay. For this transport problem we have developed an inhomogeneous nonunitary Lindblad master equation that allows for a description of open quantum systems with both sinks (electron loss) and source (capture) present. We apply this theoretical framework to study transient coherences created in electron capture by 13.6 MeV/amu Ar^{18+} ions transmitted through amorphous carbon foils and decoherence during subsequent interaction with the foil. In the limit of thin targets we can directly probe electron capture cross sections under single collision conditions, while for thicker targets we follow the partially coherent dynamics of the open quantum system in interaction with the solid as a function of interaction time. The calculated results are in close agreement with experimental data obtained at the LISE facility in GANIL. Photon intensities from excited argon ions were determined through high resolution x-ray spectroscopy in which individual fine structure components were resolved. Measurements were performed for a wide range of carbon foil thickness to study the time development of the excited state populations.

DOI: 10.1103/PhysRevA.75.032714 PACS number(s): 34.50.Fa, 34.10.+x

I. INTRODUCTION

The passage of an atom or ion through a solid involves a rich variety of inelastic electronic processes. Theoretical description of such interactions remains a challenge, in part due to large number of degrees of freedom involved. Systems of such complexity are ideal candidates for applications of open quantum system (OQS) approaches, within which only the (sub) system, in the present case the electronic degrees of freedom of the hydrogenic projectile, is treated explicitly. The rest of the system, here the solid (its electronic and ionic degrees of freedom) and the radiation field, is treated as an environment.

A theoretical description of the partially coherent evolution of the electronic system requires a generalization of previously developed OQS approaches. The starting point is the Lindblad master equation (LME). In its simplest form, frequently employed in quantum optics [1,2], it describes the unitary evolution of the system in the presence of the environment (reservoir) where the latter induces energy exchange and decoherence in the system. For the transport of projectile states in the solid, extensions beyond this standard form are necessary. The interaction with the reservoir cannot only destroy but also transiently induce coherences [3]. Moreover, electron loss (i.e., ionization) represents a net flux of probability out of the system into the environment. Such open quantum systems are not only open with respect to energy transfer but also with respect to probability flux. Enforcing unitarity means unphysical suppression of flux out of the system and thus distortion of the evolution within the truncated Hilbert space. In Ref. [4] we developed a nonunitary OQS extension to previous approaches that accounts for probability flux out of the truncated Hilbert space of the system. In the application to the projectile state evolution in the solid this approach permits explicit treatment of the low-lying states of the ion within a finite Hilbert space of manageable size accounting for the flow of probability towards highly excited bound states and continuum states. Application to transport of hydrogenic Kr^{35+} through amorphous carbon foils [4] has led to satisfying agreement with experimental data.

The present case of bare argon projectiles (Ar^{18+}) calls for a further extension [5]. Unlike Kr^{35+}, the projectile is not carrying any electron prior to entering the foil and, therefore, a coherent source of probability flux must be taken into account. Only as the projectile captures an electron (i.e., undergoes charge transfer $Ar^{18+} \rightarrow Ar^{17+}$), does the one-electron Hilbert space of the system become occupied. This feeding proceeds in a partially coherent fashion. At the same time, the one-electron Hilbert space can be depleted not only by ionization ($Ar^{17+} \rightarrow Ar^{18+}$) but also via a second capture process ($Ar^{17+} \rightarrow Ar^{16+}$). This class of processes therefore requires a generalization of the OQS description to an inhomogeneous LME with a coherent source that simultaneously acts as a sink. Development of a theoretical description is the goal of the present paper.

The present investigation is partially motivated by an outstanding discrepancy between experiment and results of clas-

*Electronic address: marek.seliger@uni-graz.at

sical transport theory (CTT) [6]. A much better agreement is obtained here owing to progress in both theory and experiment. On the theoretical side we have developed a well founded open quantum system approach with sinks and sources. In addition, since source density matrices vary substantially among different approximation methods [6,7], a considerable effort has been devoted to performing a robust calculation of electron capture in binary collisions by numerically solving on a three-dimensional lattice the time-dependent Schrödinger equation (LTDSE).

From the experimental point of view, we present here data in which the evolution of state populations of an argon projectile penetrating an amorphous carbon foil at 13.6 MeV/amu has been determined by x-ray spectroscopy. Photon intensities after foil exit have been detected at GANIL (Grand Accélérateur National d'Ions Lourds) on the LISE facility. The $2s_{1/2}$ decay and the Lyman series were measured using high resolution spectroscopy in which individual $2p \rightarrow 1s$ fine structure components could be resolved. The thinnest targets available allow study of electron capture under single collision conditions. Propagation of the projectile through targets with different thickness allows the dynamics to be followed from single collision conditions to equilibrium corresponding to a thickness of 2 to 200 $\mu g/cm^2$ ($\sim$100 Å to 1 μm) of the amorphous carbon foil. Multiple collisions with constituents of the solid and radiative decay redistribute the initial population created by electron capture.

This paper is organized as follows. In Sec. II we present the open quantum system approach and the solution by means of quantum trajectories. The implementation of our approach for the transmission of argon ions through carbon foils is described in Sec. III. The calculation of electron capture defining the initial conditions of the density matrix is reviewed in Sec. III C. A brief summary of the experimental measurement of excited states populations by means of x-ray spectroscopy is given in Sec. IV. Finally we compare experimental findings with numerical calculations of the transport problem in Sec. V. Atomic units (a.u.), where $|e|=m_e=\hbar=1$ and $c=137$, will be used throughout this paper unless stated otherwise.

II. INHOMOGENEOUS NONUNITARY LINDBLAD MASTER EQUATION

The starting point of a theoretical analysis of open quantum systems (OQSs) is, typically, the reduction of the master equation for the reduced density matrix to a Redfield equation by applying the Born-Markov approximation [1–3,8,9]. A further simplification of the relaxation superoperator leads to the Lindblad master equation [10,11]. The latter is frequently used as it can serve as a suitable starting point for quantum trajectory methods. Even with such a drastic simplification which treats the coupling to the environment in first-order perturbation theory and neglects memory effects, a solution of the equation of motion for the density matrix is still a formidable task. Difficulties in describing OQSs in terms of the evolution of the reduced density matrix originate, in part, from the high dimensionality of the problem.

In a system with N_S states the direct solution of the quantum master equation (QME) involves N_S^4 couplings. For small systems the QME can be solved directly. For a large system, such as the electronic degrees of freedom of an ion, where N_S can easily reach $N_S \approx 10^3$, a complete solution is no longer feasible. The problem can be circumvented by reducing N_S and, moreover, by reducing the number of couplings to those assumed to be the dominant ones [12]. An attractive alternative is solving the full QME by means of a Monte Carlo discretization with quantum trajectories. Propagating states rather than the density operator leads to a scaling of the solution with N_S^2. This allows treatment of large OQSs within quantum mechanics. The quantum trajectory approach requires, however, for the QME to be of the Lindblad form (or closely related to it [4]), in order to assure positive definiteness of the reduced density operator at any time. The task is thus to construct a generalized Lindblad master equation for quantum systems that are open with respect to energy and probability flux. Such an inhomogeneous Lindblad master equation (ILME) is then accessible to solutions via a quantum trajectory Monte Carlo (QTMC) technique, just as is the case for the standard LME. We begin by first briefly reviewing the standard LME (Sec. II A) and then present the extension to an inhomogeneous master equation allowing for exchange of probability flux between the system and the environment (Sec. II B). The efficient solution by means of a QTMC method is described in Sec. II C and II D.

A. Unitary Lindblad master equation

Consider a system S with Hamiltonian H_S interacting with an environment referred to in the following as the "reservoir" (R) with Hamiltonian H_R through a coupling interaction V_{SR}. In the present transport problem the environment is the solid while the system under consideration is the projectile. Later, the interaction V_{SR} will describe collisions of the projectile with constituents of the solid as well as interaction with the radiation field. The time evolution of the density matrix $\rho(t)$ of the entire interacting system is given by the Liouville-von Neumann equation

$$\frac{d}{dt}\rho(t) = -i[H,\rho(t)] \tag{2.1}$$

with the total Hamiltonian $H=H_S+H_R+V_{SR}$.

Clearly, the solution of the full Liouville-von Neumann equation is out of reach for realistic systems involving a large number of degrees of freedom. Instead, the focus is on a master equation, an equation of motion for the reduced density matrix of the system of interest $\sigma(t)$, which is obtained by tracing out all degrees of freedom of the reservoir, $\sigma(t)=\mathrm{Tr}_R[\rho(t)]$. The corresponding reduced density matrix of the reservoir would be $\sigma^R(t)=\mathrm{Tr}_S[\rho(t)]$. The reduction usually entails a number of additional approximations such as the Born-Markov approximation which neglects memory effects and treats the coupling V_{SR} in first-order perturbation theory.

The Lindblad form of a master equation (LME) describes a unitary time evolution by means of the Lindblad transition operators $S(\vec{k})$,

$$\frac{d}{dt}\sigma(t) = -i[H_S, \sigma(t)] - \frac{1}{2}\int d^3k[S^\dagger(\vec{k})S(\vec{k}), \sigma(t)]_+ + \int d^3k S(\vec{k})\sigma(t)S^\dagger(\vec{k}), \tag{2.2}$$

where the parameter $\vec{k}$ may represent a momentum transfer in collisions or the photon momentum in radiative decay. It can be discrete or continuously distributed. The Lindblad transition operators $S(\vec{k})$ are explicitly given in Ref. [3] for the different environmental interactions relevant to the present transport problem. Equation (2.2) assures the positive definiteness of $\sigma(t)$ for all times. The important consequence of this property of the Lindblad form of the master equation is the possibility to solve it by means of a QTMC technique opening up a wide range of applications.

B. Inhomogeneous nonunitary Lindblad master equation with a source

The construction of (2.2) results in the exact compensation of the loss of probability described by the anticommutator (second term: $[\ ,\ ]_+$ on the right-hand side) by the last term. Consequently, probability is conserved. The unitarity constraint

$$\frac{d}{dt}\mathrm{Tr}_S[\sigma(t)] = 0, \tag{2.3}$$

built into the Lindblad equation, poses a hurdle for realistic numerical simulations because it remains in force when the Hilbert space is truncated to dimension N_S. For realistic systems which include continuum states, a strictly unitary evolution is unphysical. Only a subspace $\mathbb{P}$ of the Hilbert space $\mathbb{H}_S$ can be represented in a numerical simulation by a truncated basis of dimension N_S. The subspace $\mathbb{P}$ is coupled to its complement $\mathbb{Q}$ by V_{SR}. The flow of probability between $\mathbb{P}$ and $\mathbb{Q}$ is therefore not an artifact but real for any computationally feasible truncated basis set. The point to be noted is that $\mathbb{Q}$ refers here to a subspace of the system Hilbert space, not to the reservoir.

The bilinear form of the transition operators S and $S^\dagger$ in the LME

$$\Gamma^{\mathbb{P}}_{\alpha\beta} = \int d^3k \Gamma^{\mathbb{P}}_{\alpha\beta}(\vec{k}) = \int d^3k \sum_\mu S^\dagger_{\alpha\mu}(\vec{k})S_{\mu\beta}(\vec{k}) \tag{2.4}$$

corresponds to the decay operator $\Gamma^{\mathbb{P}}$ for the states α and β via all intermediate states μ, where α and β are elements of $\mathbb{P}$. They will, however, couple also to states outside $\mathbb{P}$. μ spans the entire Hilbert space $\mathbb{H}_S = \mathbb{P} \oplus \mathbb{Q}$. The decay operator can thus be decomposed as

$$\Gamma^{\mathbb{P}}_{\alpha\beta}(\vec{k}) = \sum_{\mu \in (\mathbb{P}\oplus\mathbb{Q})} S^\dagger_{\alpha\mu}(\vec{k})S_{\mu\beta}(\vec{k}) = \Gamma^{\mathbb{PP}}_{\alpha\beta}(\vec{k}) + \Gamma^{\mathbb{PQ}}_{\alpha\beta}(\vec{k}). \tag{2.5}$$

$\Gamma^{\mathbb{PP}}_{\alpha\beta}(\vec{k})$ describes transitions within the subspace $\mathbb{P}$ with $\mu \in \mathbb{P}$ while outward probability flux is described by the decay operator for loss

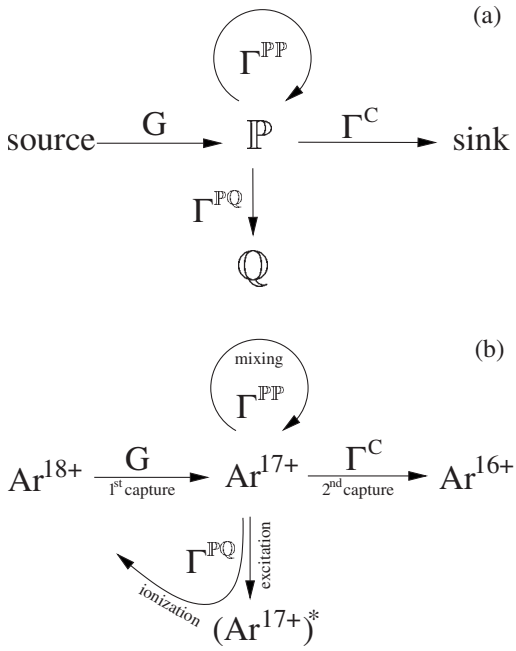

FIG. 1. Schematic picture of the terms entering the Lindblad master equation (a) and on the example of argon transport (b).

$$\Gamma^{\mathbb{PQ}}_{\alpha\beta}(\vec{k}) = \sum_{\mu\in\mathbb{Q}} S^\dagger_{\alpha\mu}(\vec{k})S_{\mu\beta}(\vec{k}). \tag{2.6}$$

$\Gamma^{\mathbb{PQ}}$ causes an explicitly nonunitary evolution within $\mathbb{P}$ since it contributes to the anticommutator in the LME (2.2) but not to the last term, which would compensate the loss of probability. The coupling to the orthogonal complement, i.e., to electronic states not within $\mathbb{P}$, is, however, not the only process that causes change of probability (Fig. 1).

Flux into $\mathbb{P}$ occurs in the present case by electron transfer from the target (the reservoir) to the projectile with amplitude, $T_{\alpha i}$, where i represents an electronic state index of the reservoir and $\alpha \in \mathbb{P}$. Because this amplitude is controlled by the occupation in the target (σ^R assumed to be stationary) rather than by σ, its inclusion into the equation of motion for σ adds an inhomogeneity to the LME in terms of a source (or gain) density matrix G with elements

$$G_{\alpha\beta} = \sum_i G^{(i)}_{\alpha\beta} = \sum_i T_{\alpha i}T^\dagger_{\beta i} = \mathrm{Tr}_R[T_{\alpha i}T^\dagger_{\beta i}], \tag{2.7}$$

where the trace is taken over electronic degrees of freedom in the target. Details of the calculation of the capture amplitudes will be given below. The key point is that capture generates and replenishes the partly coherent population of $\mathbb{P}$. In particular, Eq. (2.7) specifies the initial density matrix σ for an Ar^{17+} ion. For fermions the gain term must be modified by the one-electron Pauli blocking term

$$G_{\alpha\beta} \to G_{\alpha\beta}(1 - \mathrm{Tr}[\sigma]). \tag{2.8}$$

Capture represents not only a gain channel but also a loss channel. The latter follows from the fact that capture of an additional electron transforms the hydrogenic system into a heliumlike system ($Ar^{17+} \to Ar^{16+}$), thus removing it from the one-electron Hilbert space $\mathbb{H}_S$ or $\mathbb{P}$. The LME (2.2) must be

amended by an anticommutator of the form representing capture-mediated probability loss from the one-electron Hilbert space,

$$-\tfrac{1}{2}[\Gamma^c,\sigma(t)]_+, \tag{2.9}$$

where

$$\Gamma^c_{\alpha\beta}=\sum_{ij}\tilde{T}_{ij}(\alpha)\tilde{T}^{\dagger}_{ij}(\beta). \tag{2.10}$$

In Eq. (2.10) $\tilde{T}_{ij}(\alpha)$ denotes the amplitude for a transition of an electron of the reservoir into a heliumlike state j of the projectile. This capture amplitude for the second electron may depend on state (α,β) of the hydrogenic (first) electron present at the instant of the capture. In a strict independent particle model for capture the dependence of the amplitude on the state index (α,β) drops out and Γ^c becomes proportional to the unit matrix in $\mathbb{P}$.

Summarizing, the generalized ILME becomes

$$\frac{d\sigma(t)}{dt}=-i[H_S,\sigma(t)]+\int d^3kS(\vec{k})\sigma(t)S^{\dagger}(\vec{k})-\frac{1}{2}[\Gamma^{\mathrm{PP}},\sigma(t)]_+ -\frac{1}{2}[\Gamma^{\mathrm{PQ}},\sigma(t)]_+-\frac{1}{2}[\Gamma^c,\sigma(t)]_++G(1-\mathrm{Tr}[\sigma(t)]). \tag{2.11}$$

For the solution of Eq. (2.11) the unitarity constraint [Eq. (2.3)] no longer applies but is replaced by the inequality

$$0\le \mathrm{Tr}[\sigma(t)]\le 1. \tag{2.12}$$

We note that for a nonunitary density operator the measure for partial coherence is given by

$$\frac{\mathrm{Tr}[\sigma^2(t)]}{(\mathrm{Tr}[\sigma(t)])^2}\le 1, \tag{2.13}$$

where the equality holds for a fully coherent state. It should be noted that the Markov approximation assumes that the reservoir is not affected by the interaction with the OQS and thus remains unchanged, i.e., $\sigma^R(t)\to\sigma^R(t=0)\to\sigma^R$. In the present case with probability flux from the reservoir to the system (and back) this assumption implies that charge transfer does not significantly alter the reservoir (the solid), i.e., an "inexhaustible" supply of electrons is not only available for charge transfer but also for screening of the holes left behind.

C. Quantum trajectory Monte Carlo solution

The popularity of the Lindblad master equation is, in part, due to the fact that it can be mapped without further approximation onto a nonlinear stochastic Schrödinger equation (NLSSE) which can be solved by propagating a Monte Carlo ensemble of state vectors: i.e., using the quantum trajectory Monte Carlo [3] or Monte Carlo wave function method [1,2,8,9]. The Lindblad master equation can be solved by an ensemble average over quantum trajectories as

$$\sigma(t)=\frac{1}{N_{\mathrm{traj}}}\sum_{\eta=1}^{N_{\mathrm{traj}}}|\Psi^{\eta}(t)\rangle\langle\Psi^{\eta}(t)|, \tag{2.14}$$

where the index η labels one particular stochastic realization (a quantum trajectory) and N_{traj} is the number of quantum trajectories controlling the statistical uncertainty. In the limit $N_{\mathrm{traj}}\to\infty$, the ensemble average can be shown to be strictly equivalent to the solution of the original Lindblad equation [13].

The time evolution of each trajectory is governed by the NLSSE,

$$|d\Psi^{\eta}(t)\rangle=\left(-iH_Sdt-\frac{dt}{2}(\Gamma^{\mathrm{PP}}+\Gamma^{\mathrm{PQ}}+\Gamma^c-\langle\Gamma^{\mathrm{PP}}\rangle_{t,\eta})+\int d^3kdN^{\eta}_k(t)[S(\vec{k})\langle\Gamma^{\mathrm{PP}}(\vec{k})\rangle^{-1/2}_{t,\eta}-1]\right)|\Psi^{\eta}(t)\rangle+\sum_{g,i}dM^{(i)\eta}_g(t)|X^{(i)}_g\rangle. \tag{2.15}$$

The terms in (2.15) proportional to dt (first line) correspond to continuous changes of the wave function $|\Psi^{\eta}(t)\rangle$. Because the right-hand side of (2.15) explicitly depends on the expectation value $\langle\Gamma^{\mathrm{PP}}(\vec{k})\rangle_{t,\eta}=\langle\Psi^{\eta}(t)|\Gamma^{\mathrm{PP}}(\vec{k})|\Psi^{\eta}(t)\rangle/\langle\Psi^{\eta}(t)|\Psi^{\eta}(t)\rangle$ of the decay operator $\Gamma^{\mathrm{PP}}(\vec{k})$, the equation is nonlinear. The variable $N^{\eta}_{\vec{k}}(t)$ counts the number of jumps for a given quantum trajectory η and a given parameter $\vec{k}$ as a function of time t starting with $N^{\eta}_k(t=0)=0$. The Ito differential, $dN^{\eta}_k(t)=N^{\eta}_k(t+dt)-N^{\eta}_k(t)$, takes, for a given quantum trajectory η and an infinitesimally short time interval dt, the value 1 when a jump occurs and 0 when it does not. This stochastic variable generates different realizations of quantum trajectories labeled by η and accounts for the stochastic transitions induced by the interactions with the environment described by Γ^{PP} (excitations and radiative decay). Since the Lindblad equation (2.11) contains an inhomogeneity, the corresponding NLSSE contains a second Ito differential dM accounting for the stochastic process of capture. The structure of this term is different due to the inhomogeneous term proportional to G in the LME (2.11).

To construct the source term for the NLSSE we first diagonalize the source density matrix $G^{(i)}$ (2.7) by means of the normalized eigenvectors $X^{(i)}_g$ for the source channel (i) with eigenvalues $x^{(i)}_g$,

$$G^{(i)}=\sum_g|X^{(i)}_g\rangle x^{(i)}_g\langle X^{(i)}_g|. \tag{2.16}$$

Expressed in terms of matrix elements in the α basis of the system it reads

$$G_{\alpha\beta}=\sum_i G^{(i)}_{\alpha\beta}=\sum_g\sum_i x^{(i)}_g X^{(i)}_{\alpha g}X^{(i)\dagger}_{\beta g} \tag{2.17}$$

with $\langle\alpha|X^{(i)}_g\rangle=X^{(i)}_{\alpha g}$.

The reduced density matrix calculated as the Monte Carlo average over a large number of stochastic realizations (2.14) yields the Lindblad equation (2.11) when the expectation

value of the Ito differentials for the system in state $|\Psi^{\eta}(t)\rangle$ at time t is properly chosen. For $dN_k^{\eta}(t)$ we impose the condition

$$\overline{dN_k^{\eta}(t)dN_{k'}^{\eta}(t)} = \overline{dN_k^{\eta}(t)}\,\delta_{\vec{k}\vec{k}'} = dt\langle\Gamma^{\mathrm{PP}}(\vec{k})\rangle_{t,\eta}\delta_{\vec{k}\vec{k}'}, \tag{2.18}$$

expressing the fact that at most one jump can happen in an infinitesimally short time interval dt with an average rate $\langle\Gamma^{\mathrm{PP}}(\vec{k})\rangle_{t,\eta}$.

Likewise the stochastic variable $dM_g^{(i)\eta}(t)$ counts the number of feeding events from a reservoir state i into a system eigenstate g of the capture process along a stochastic trajectory. Its initial value is set to $M_g^{(i)\eta}(t=0)=0$. This Ito differential satisfies the condition

$$\begin{aligned}\overline{dM_g^{(i)\eta}(t)dM_{g'}^{(j)\eta}(t)} &= \overline{dM_g^{(i)\eta}(t)}\,\delta_{gg'}\delta_{ij} \\ &= \delta_{gg'}\delta_{ij}dt x_g^{(i)}(1-\mathrm{Tr}[\sigma(t)]),\end{aligned} \tag{2.19}$$

where the index i runs over all occupied states in the target and unobserved degrees of freedom such as the impact parameter of the collision. We assume the electronic degree of freedom of the target to be in the fermionic ground state and that the depletion of the reservoir by previous capture events can be neglected.

D. Calculation of quantum trajectories

Within the present formalism the density matrix can be calculated as

$$\sigma(t) = \frac{1}{N_{\mathrm{traj}}}\int_0^t dt_0 \sum_{i,g} p_{i,g}(t_0)\sum_{\eta=1}^{N_{\mathrm{traj}}} |\Psi^{\eta,i,g,t_0}(t)\rangle\langle\Psi^{\eta,i,g,t_0}(t)|, \tag{2.20}$$

where $p_{i,g}(t_0)=x_g^{(i)}(1-\mathrm{Tr}[\sigma(t_0)])$ is the rate per unit time that the state $|X_g^{(i)}\rangle$ is created at the time t_0 as the result of an electron capture event. [In practice, the integral over t_0 represents a convolution and the sum over i and g is calculated using a Monte Carlo method and the final result resembles Eq. (2.14) with $\eta\to\eta,i,g,t_0$.]

The time evolution of each quantum trajectory is constructed by applying the time evolution operator to the initial state

$$|\Psi^{\eta,i,g,t_0}(t)\rangle = U^{\eta}(t,t_0)|X_g^{(i)}\rangle. \tag{2.21}$$

The initial state is populated by a stochastic feeding (capture) process generating the state $|X_g^{(i)}\rangle$ at time t_0. Subsequently, as long as no further capture takes place, $|\Psi^{\eta}(t)\rangle$ evolves according to the NLSSE without a source

$$|d\Psi^{\eta}(t)\rangle = \left(-iH_S dt - \frac{dt}{2}(\Gamma^{\mathrm{PP}}+\Gamma^{\mathrm{PQ}}+\Gamma^{c}-\langle\Gamma^{\mathrm{PP}}\rangle_{t,\eta}) + \int d^3k dN_k^{\eta}(t)[S(\vec{k})\langle\Gamma^{\mathrm{PP}}(\vec{k})\rangle_{t,\eta}^{-1/2}-1]\right)|\Psi^{\eta}(t)\rangle \tag{2.22}$$

which is (when omitting Γ^c) described in detail in Ref. [4].

The time evolution operator in Eq. (2.21) is constructed as a sequence of continuous time evolution operators and discontinuous jump operators as

$$U^{\eta}(t,t_0) = U_{\mathrm{cont}}^{\eta}(t,t_n)\prod_{j=1}^{n} U_{\mathrm{jump}}^{\eta}(\vec{k}_j,t_j)U_{\mathrm{cont}}^{\eta}(t_j,t_{j-1}). \tag{2.23}$$

The application of the continuous time evolution operator

$$|\Psi^{\eta}(t_j)\rangle = U_{\mathrm{cont}}^{\eta}(t_j,t_{j-1})|\Psi^{\eta}(t_{j-1})\rangle \tag{2.24}$$

results in

$$|\Psi^{\eta}(t_j)\rangle = ||\Psi^{\eta}(t_{j-1})||\frac{e^{-i[H_S-(i/2)(\Gamma^{\mathrm{PP}}+\Gamma^{\mathrm{PQ}}+\Gamma^{c})]\Delta t}}{||e^{-i[H_S-(i/2)\Gamma^{\mathrm{PP}}]\Delta t}|\Psi^{\eta}(t_{j-1})\rangle||}|\Psi^{\eta}(t_{j-1})\rangle \tag{2.25}$$

with the time difference $\Delta t=t_j-t_{j-1}$. The flow of probability out of $\mathbb{P}$ is realized by the continuous time evolution operator $U_{\mathrm{cont}}^{\eta}(t_j,t_{j-1})$ in (2.25) where we use decay operators $\Gamma^{\mathrm{PP}}+\Gamma^{\mathrm{PQ}}+\Gamma^{c}$ in the numerator and only Γ^{PP} in the denominator. The loss of norm is caused by $\Gamma^{\mathrm{PQ}}+\Gamma^{c}$ which appears only in the continuous propagation in time, $U_{\mathrm{cont}}^{\eta}(t_j,t_{j-1})$, without a counter term in the jump operator. Application of the jump operator

$$\begin{aligned}|\Psi^{\eta}(t_j+\delta t)\rangle &= U_{\mathrm{jump}}^{\eta}(\vec{k}_j,t_j)|\Psi^{\eta}(t_j)\rangle \\ &= ||\Psi^{\eta}(t_j)||\frac{S(\vec{k}_j)}{||S(\vec{k}_j)|\Psi^{\eta}(t_j)\rangle||}|\Psi^{\eta}(t_j)\rangle\end{aligned} \tag{2.26}$$

describes transitions within $\mathbb{P}$ leaving the norm unchanged.

The resulting density matrix in Eq. (2.20) can be rewritten as

$$\sigma(t) = \frac{1}{N_{\mathrm{traj}}}\sum_{\eta}\sum_{g}\sum_{i}\int_0^t dt_0 U^{\eta}(t,t_0)|X_g^{(i)}\rangle\langle X_g^{(i)}|U^{\eta\dagger}(t,t_0) \times \frac{\overline{dM_g^{(i)\eta}(t_0)dM_g^{(i)\eta}(t_0)}}{dt_0}. \tag{2.27}$$

Using Eq. (2.19) and $U^{\eta}(t,t_0)=U^{\eta}(t-t_0,0)$,

$$\sigma(t) = \int_0^t dt_0\{1-\mathrm{Tr}[\sigma(t_0)]\}\tilde{\sigma}(t-t_0) \tag{2.28}$$

with

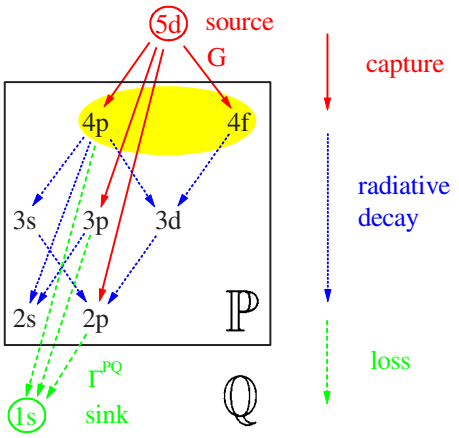

FIG. 2. (Color online) Model system of radiative cascade of a hydrogenic argon ion initially in the $5d_{3/2,1/2}$ state in the OQS approach. Solid lines, gain of probability; long dashed lines, internal radiative transitions within the subspace $\mathbb{P}$ of states within the box; short dashed lines, loss to the complement subspace $\mathbb{Q}$.

$$\tilde{\sigma}(t') = \frac{1}{N_{\text{traj}}} \sum_{\eta} U^{\eta}(t',0) G U^{\eta\dagger}(t',0). \tag{2.29}$$

The interpretation of Eqs. (2.28) and (2.29) is as follows. $\tilde{\sigma}(t')$ would correspond to the solution of a LME by an ensemble of trajectories in the absence of a source [see Eq. (2.11)] where G would represent the initial conditions, i.e.,

$$\tilde{\sigma}(t'=0) = G. \tag{2.30}$$

It should be noted that additional capture events during the time interval $[t_0,t]$ are included in terms of the effective loss operator Γ^c in (2.25). Equation (2.28) represents, in turn, the sum (average) over all propagated capture density matrices initialized at different capture times t_0 weighted by the "blocking factor" $\{1-\mathrm{Tr}[\sigma(t_0)]\}$ which expresses the fact that capture at t_0 is suppressed when the one-electron Hilbert space is already occupied (Pauli blocking). Finally, taking the trace over (2.28) results in an implicit equation

$$\mathrm{Tr}[\sigma(t)] = \int_0^t dt_0 \{1 - \mathrm{Tr}[\sigma(t_0)]\} \mathrm{Tr}[\tilde{\sigma}(t-t_0)] \tag{2.31}$$

for the time-dependent norm of the nonunitary density operator.

III. IMPLEMENTATION FOR RADIATIVE DECAY AND ION-SOLID INTERACTIONS

A. Radiative cascade

We first implement and apply the newly developed method to a model system where an exact solution for the entire system ($\mathbb{H}_S$) is available against which we can test the present algorithm for the subspace $\mathbb{P}$. For this purpose we consider the cascade from a state radiatively decaying into the ground state. The model system we analyze is an excited hydrogenic argon ion initially in the $5d_{3/2,1/2}$ state as shown in Fig. 2. We artificially decompose the Hilbert space into three subspaces: (i) the subspace containing the initial state serving as a source of probability, (ii) the simulated subspace $\mathbb{P}$ spanning states reached directly by radiative transitions from the initial state, i.e., all states within the shells $n=2$, 3, and 4, and (iii) the complement subspace $\mathbb{Q}$ playing the role of the sink which is here the ground state ($1s$). We compare the ILME for the time evolution within the reduced space $\mathbb{P}$ within which the radiative decay of the initial state is treated as an environmental source term G and the decay into the ground state as loss to the complement with the direct solution of the unitary LME within the larger space ($\mathbb{H}_S$) including the initial and ground states.

The radiative decay enters the ILME (2.11) in three terms: (i) a source term G feeding $\mathbb{P}$, (ii) as internal transitions within $\mathbb{P}$ (via Γ^{PP} and S) and (iii) as loss $\mathbb{P}\to\mathbb{Q}$ (via Γ^{PQ}). The decay of the initial state representing the source term G is constructed from the transition operators $S_{ij}^{(r)}(\mathfrak{I})$ [3] describing radiative decay for the polarization directions $\mathfrak{I}=x,y$, and z as,

$$G_{\alpha\beta}(t) = \sum_{\mathfrak{I}}^{xyz} S_{\alpha i}^{(r)}(\mathfrak{I}) S_{\beta i}^{(r)*}(\mathfrak{I}) \sigma_{ii}^{R}(t), \tag{3.1}$$

with the initial state $i=5d_{3/2,1/2}$. Equation (3.1) describes both the growth of population [diagonal elements of $\sigma(t)$] as well as build-up of coherences in the off-diagonal elements of $\sigma(t)$. Unlike the case of a truly open quantum system coupled to a large reservoir which we will consider below for ion-solid collisions, we account in the present test case for the depletion of the reservoir,

$$\sigma_{ii}^{R}(t) = e^{-\mathrm{Tr}[S^{(r)}S^{(r)*}]t} \sigma_{ii}^{R}(t=0), \tag{3.2}$$

which corresponds to an exponential decay of the state i with the rate $\mathrm{Tr}[SS^*]$. The initial population $\sigma_{ii}^{R}(t=0)$ of the source term is set to one resulting in a source term in the ILME

$$G_{\alpha\beta}(t) = \sum_{\mathfrak{I}}^{xyz} S_{\alpha i}^{(r)}(\mathfrak{I}) S_{\beta i}^{(r)*}(\mathfrak{I}) e^{-\mathrm{Tr}[SS^*]t}. \tag{3.3}$$

In this particular case of a one-electron system, blocking terms of the form $(1-\mathrm{Tr}[\sigma(t_0)])$ do not appear and $\Gamma^c=0$.

As a sensitive test case for the inhomogeneous Lindblad equation we compare its prediction with an exact solution for the transient build-up and decay of coherences between the $4p_{3/2}$ and $4f_{5/2}$ states due to radiative transitions (Fig. 3). This exact solution is obtained via the LME where $\mathbb{P}$ spans over all relevant subspaces, i.e., $n\leq 5$. For short times the coherence $\sigma_{\alpha\beta}$ increases exponentially according to $1-\exp(-S_{\alpha i}^{(r)} S_{\beta i}^{(r)*} t)$ with the corresponding gain rate $S_{\alpha i}^{(r)} S_{\beta i}^{(r)*}$ as indicated in Fig. 3. For longer times, transitions within the subspace $\mathbb{P}$ and loss to $\mathbb{Q}$ result in beats and the decay of the coherence density matrix elements. The agreement between the ILME and the exact solution is, to within the graphical resolution, perfect thus lending support to the validity and accuracy of the present approach to open quantum systems with sources and sinks.

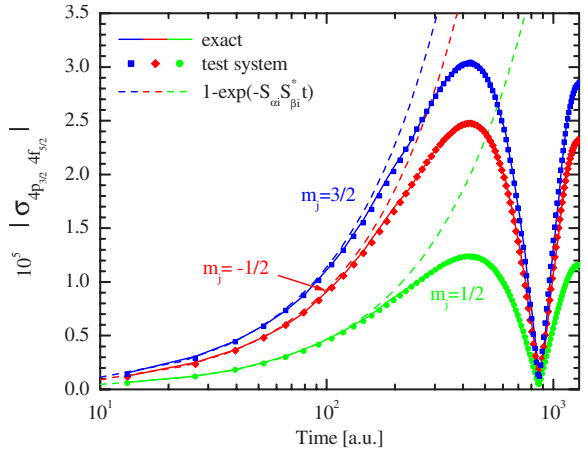

FIG. 3. (Color online) Absolute magnitude of coherence between the Ar^{17+} states $4p_{3/2,m_j}$ and $4f_{5/2,m_j}$ for $m_j=-1/2,1/2$, and 3/2 populated by radiative decay from $5d_{3/2,1/2}$. Solid lines, exact calculation; symbols, calculation according to the ILME for the system displayed in Fig. 2; dashed lines, exponential increase.

B. Ion-solid interaction

We apply the open quantum system approach next to the transport of electronic states of highly charged ions penetrating solids. We focus on bare argon ions (Ar^{18+}) with a velocity of $v_p=23$ a.u. traversing thin amorphous carbon foils. One interesting feature of this class of transport problems is that the environmental interaction is switched on suddenly when the projectile enters the solid and ceases suddenly after exiting the solid, thus allowing the time-resolved study of the evolution of the internal state of ions on an attosecond to femtosecond time scale.

The evolution of projectile states traveling through a solid is obviously a complex problem due to the many-body dynamics involved. To gain insight into the dynamics we subdivide the target into its individual constituents and consider their interaction with the projectile. The solid is composed of ionic cores and electrons bound to these cores. The relevant processes in ion-solid transport can be divided into two groups: exchange of energy and momentum with the solid and exchange of constituents. The latter consists of electron capture from the target to the projectile and the inverse process, transfer of electrons from the projectile to the target.

The Hamiltonian of the system outside the foil is the unperturbed hydrogenic Hamiltonian

$$H_S = -\nabla_r^2/2 - Z_p/r + \Delta H_{\mathrm{rel}} \tag{3.4}$$

including relativistic corrections ΔH_{rel}, i.e., for the fine structure and the Lamb shift. Eigenstates of H_S can be described by the quantum numbers n,l,j, and m_j.

The system Hamiltonian inside the solid contains additionally the contribution from the wake field [14,15] as

$$H_S^{(\mathrm{solid})} = H_S + V^{(w)}, \tag{3.5}$$

which is the target polarization induced by the high nuclear charge of the projectile. We employ a sudden approximation for the transition from H_S to $H_S^{(\mathrm{solid})}$ at the foil entrance at which the interaction $V^{(w)}$ is switched on. Likewise, we switch off $V^{(w)}$ at the exit surface and project onto atomic final states in vacuum (eigenstates of H_S) invoking, again, a sudden approximation. The interaction with the environment includes scattering at the ionic cores, $\Gamma^{\mathrm{P(c)}}$, scattering at the electron gas, $\Gamma^{\mathrm{P(e)}}$, and radiative decay $\Gamma^{(\mathrm{r})}$. The total decay operator is thus

$$\Gamma^{\mathrm{P}} = \Gamma^{\mathrm{P(c)}} + \Gamma^{\mathrm{P(e)}} + \Gamma^{(\mathrm{r})}. \tag{3.6}$$

Details can be found in Ref. [3]. Ionization, described by Γ^{PQ}, is discussed in detail in Ref. [4].

In contrast to previous studies we include here charge transfer from the target to the projectile, accounting for the presence of a source. Since the relevant projectile velocity is high ($v_p=23$ a.u.) charge transfer is significant only from the 1s shell of carbon. Therefore, we treat the electron capture by an initially fully stripped ion (Ar^{18+}) from the $1s$ shell of carbon. Within the independent electron model [16] the double occupancy of the $1s$ shell is accounted for by multiplying the charge transfer probabilities by a factor 2. Accordingly, the source term reads

$$G_{\alpha\beta}(t) = 2n_A v_p\, \mathrm{Tr}[T_{\alpha,C(1s)} T^*_{\beta,C(1s)}](1 - \mathrm{Tr}[\sigma(t)]), \tag{3.7}$$

where the current of particles per unit time is expressed as a product of the number density of the target atoms n_A and the projectile velocity v_p. The product $T_{\alpha,C(1s)}T^*_{\beta,C(1s)}$ is the capture density matrix for capture from the $1s$ orbital to the projectile orbitals (α,β), whose diagonal elements are the collisional cross sections [7]. The trace in (3.7) extends over unobserved degrees of freedom, here the impact parameter of the Ar-C collision.

We assign the various terms of the ILME to the following processes: the system space $\mathbb{P}$ consists of all bound states of Ar^{17+} up to $n_{\max}=4$. We estimate the population of higher excited states up to $n=10$ by extrapolation of the n,l,m distributions using scaling properties drawn from classical transport theory [6,17–19]. Ionization ($Ar^{17+}\rightarrow Ar^{18+}$) as well as excitation to high-lying excited states are described by Γ^{PQ}. G describes the electron capture channel converting Ar^{18+} ions into Ar^{17+} ions. Additional capture, ($Ar^{17+}\rightarrow Ar^{16+}$), is neglected since its probability during the propagation distance considered in the experiment is small.

C. Calculation of the source term

The transfer of an electron from a carbon atom to the impinging argon ion may be treated through a number of approximations. Common approaches are the continuum distorted-wave (CDW) approximation [20–23] and the classical trajectory Monte Carlo (CTMC) method [24–28]. Experience shows that CDW and CTMC results agree reasonably well for charge transfer in many ion-atom collision systems regarding the total and n-level resolved cross sections for the dominant channels but, typically, do not agree as well for ℓ-resolved cross sections.

The situation is even less clear for coherences, i.e., off-diagonal elements of the density matrix. Which of the two approaches yields a more realistic input in the present case of Ar-C collisions is not readily predictable. Therefore, in order

to test which approximation is better suited for the present system, we have performed a benchmark calculation by employing the lattice time-dependent Schrödinger equation (LTDSE) approach [7,29–31]. For computational convenience, we focus on $n \leq 3$ and use the LTDSE approach to provide clues as to the validity of CDW or CTMC which we, then, extrapolate to higher n-levels. In the LTDSE approach the electronic wave function and the operators (i.e., kinetic and potential energy) are represented on a numerical grid. The wave function is then propagated in time and analyzed to yield, for example, channel-resolved charge transfer probabilities. The method has recently been described in detail in Ref. [7]. That work also introduced a hybrid approach augmenting the LTDSE treatment of the problem within a relatively small spatial grid surrounding the distance of closest approach between the target and projectile, where the interaction is strongest and most complex, with time propagation through an atomic-orbital close-coupling (AOCC) expansion involving only the very small number of bound states needed in the space outside this inner region.

Here we have adapted the LTDSE-AOCC method [7] to describe the collision of Ar^{18+} with a carbon atom. In order to represent the screening of the nuclear charge experienced by the one active electron due to the other electrons in carbon, we use a parametrized Hartree-Fock model potential [32,33] to describe the interaction of the electron with the carbon core. We also adopt the so-called semiclassical approximation in which the projectile trajectory is a straight line, representing a very good approximation given the relatively high velocity considered here.

The grid consists of 320^3 knot points and extends from -3.32 to 3.32 a.u. in each of the three Cartesian directions, resulting in a linear mesh spacing 4 times smaller than the Ar^{17+} $(1s)$ radial expectation value. A Fourier representation of the derivative operators was adopted as in previous work [7] yielding an optimal representation for the given number of knots. The potential was softened near the electronic radial distance $r=0$ (i.e., $r \to \sqrt{r^2+s}$). By performing repeated eigensolution of the lattice Hamiltonian with variation of the "softcore" parameter s, its value is chosen and fixed by matching the Hartree-Fock expectation value of energy for $C(1s)$. A value of $s=7.36\times10^{-6}$ for carbon yielded $\langle E\rangle = -11.326$ a.u. Similarly, a softcore parameter for the projectile-electron Coulombic interaction of 4.526×10^{-5} gave $\langle E\rangle=-162$ a.u. for $Ar^{17+}(1s)$. With the softcore parameters fixed, partial diagonalization of the lattice Hamiltonian yielded wave functions for the deeply bound states of Ar^{17+} for $n=1,2,3$ that were needed in analysis of subsequent stages of the calculation, and analytic wave functions were computed for projection onto the states in the $n=4$ and 5 manifolds.

In order to localize the electronic probability density after charge transfer to the center of the numerical grid, calculations were performed in the projectile frame. The carbon atom was placed at an initial distance of -2.515 a.u. from the Ar^{18+} ion along the z direction, referred to the origin of coordinates at the center of the cubic grid. This internuclear separation was well beyond the radial expectation value of the $C(1s)$ state on the grid ($\langle r\rangle \sim 0.27$ a.u.) and not overlapping with the complex absorbing potential near the edge of the grid (see Ref. [7]). The split operator method was then used to propagate the carbon atom past the ion along a straight line, for various impact parameters ranging from $b=0.01$ to 0.65 a.u., up to a distance of $z=+2.515$ a.u. (with a time step of 8.725×10^{-5} a.u.). At that point the time-evolved wave function was projected onto the set of eigenstates of Ar^{17+} and the resulting amplitudes were used to seed the extended AOCC time propagation which was carried out including the projectile bound states of interest. A number of tests indicated that the charge transfer probabilities (or density matrix elements) were converged with respect to internuclear distance (or equivalently, propagation time) already at the conclusion of the lattice calculation owing to the high velocity of the collision and the small dipole moment $\sim n^2/Z_p$ of the highly charged ion [34].

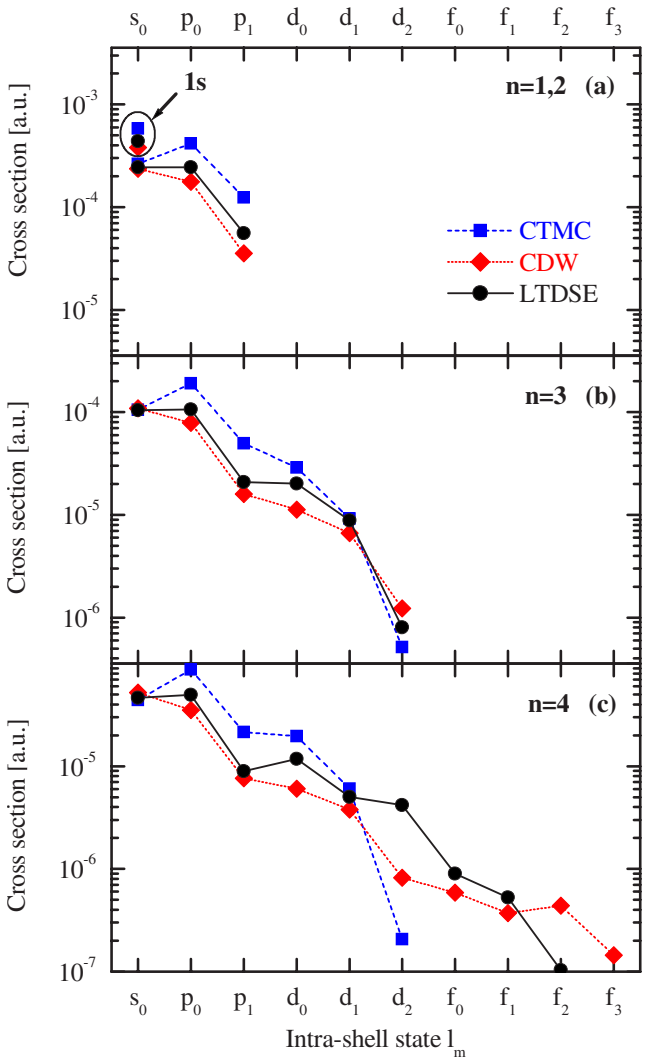

FIG. 4. (Color online) State selective charge transfer cross sections computed using the LTDSE (●), CDW (◆), and CTMC (■) approaches for $Ar^{18+}+C$ at a projectile velocity of 23 a.u. for different shells: $n=1$ and $n=2$ (a); $n=3$ (b); and $n=4$ (c).

Figure 4 presents a comparison of the LTDSE results with those from our CDW and CTMC calculations. For the states within the $n \leq 3$ manifolds, the LTDSE results lie in between

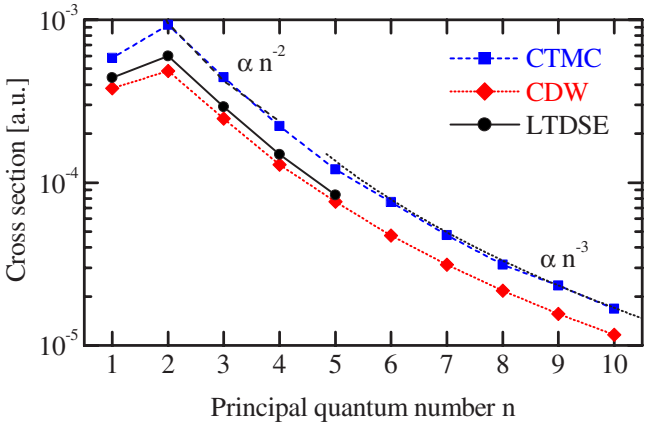

FIG. 5. (Color online) Cross sections for $Ar^{18+}+C \rightarrow (Ar^{17+})^* + C^+$ collisions at $v_p=23$ a.u. for electron capture into different shells within different approximations [CTMC (■); CDW (◆); and LTDSE (•)]. The scaling with n for results obtained with CTMC is indicated for small n as $\propto n^{-2}$ (dashed line) and in the limit of high n as $\propto n^{-3}$ (dotted line).

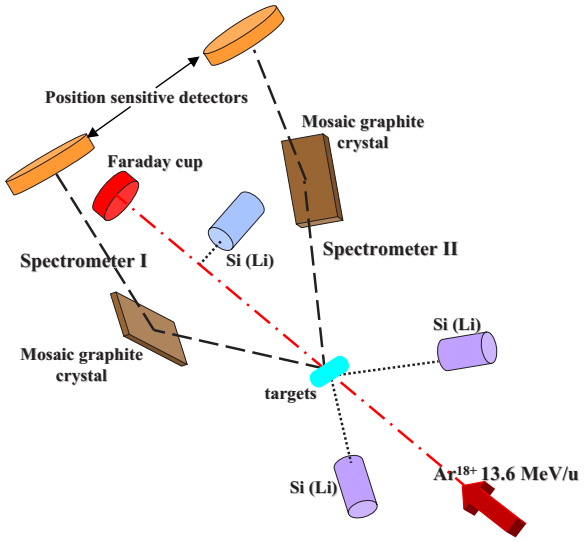

FIG. 6. (Color online) Schematic illustration of the experimental arrangement.

those from CDW and CTMC, with CTMC practically always above LTDSE and CDW always below. On average, CDW is somewhat closer to the LTDSE than is CTMC for the dominant np cross sections. Therefore, we choose CDW as the approximation to include the higher n levels for the present collision system. For $n=4$, the LTDSE show a very similar pattern in comparison to CDW and CTMC as for $n=3$, except for the f states, where they decrease with increasing m_l much faster than CDW. Regarding the behavior of the capture cross section summed over l and m_l, capture into $n=2$ is strongest and drops off rapidly for higher shells (Fig. 5). This decrease is first proportional to n^{-2} for lower n and n^{-3} for higher n. This feature is reproduced by all three approaches.

A more sensitive test is provided by the real and imaginary parts of the off-diagonal density matrix elements, which, in addition, are important input quantities for the transport simulation. The three approaches agree for the relative magnitudes and phases, with the LTDSE results again lying generally between those of CTMC and CDW and more closely to CDW than to CTMC. Table I shows intrashell coherences for the LTDSE and CDW results, with CTMC omitted for clarity of the display, for the $n=2$ and $n=3$ manifolds. The differences between LTDSE and CDW are typically quite small, the largest difference being about 30%.

This observation is particularly interesting and somewhat surprising since for charge transfer in p-He collisions, CTMC has proven to be more accurate than the CDW approximation [7]. We suspect the origin to lie in the different spatial extent of the wave functions. Charge transfer via delocalized wave functions of lower charged ions appears to be better described within a classical sampling of the phase space (CTMC) than by a perturbation treatment (CDW). For highly charged ions the electronic wave functions are more localized at the vicinity of the nucleus and consequently a perturbation treatment within the CDW approximation is expected to perform better than the classical calculation.

IV. EXPERIMENT

The experiment described here gives access, with a high accuracy, to the evolution of the population of Ar^{17+} excited states in transport through a solid. It has been performed on the LISE (Ligne d'Ions Super Epluchés) facility at GANIL (Grand Accélérateur National d'Ions Lourds - Caen, France). The setup is depicted schematically in Fig. 6 where 13.6 MeV/amu fully stripped Ar^{18+} ions are directed onto either solid foils or gaseous targets. The beam intensity, in the range 10–800 nA e, is measured by a Faraday cup allowing to obtain the number of ion projectiles (N_{proj}) with a typical precision better than 1%. Fourteen self-supported carbon foils of thickness ranging from 2.1 (±30%) to 160

TABLE I. Intrashell coherences of the electron capture density matrix for a bare Ar^{18+} ion colliding with a carbon atom ($v_p=23$ a.u.) in atomic units $\times 10^{-5}$ (1 a.u. corresponds to 2.8×10^{-17} cm^2) calculated by different methods (CDW and LTDSE) for the $n=2$ and $n=3$ manifolds.

	CDW	LTDSE
$2s_0\ 2p_0$	$2.525+i17.15$	$2.243+i20.04$
$3s_0\ 3p_0$	$1.455+i7.868$	$1.404+i8.936$
$3s_0\ 3d_0$	$-1.904+i0.711$	$-2.582+i0.789$
$3p_0\ 3d_0$	$0.314+i2.568$	$0.475+i4.196$
$3p_{\pm1}\ 3d_{\pm1}$	$0.054+i0.829$	$0.021+i1.275$

TABLE II. Energy of observed lines in eV with the global transmission T_{np} and T_{2s} for each type of detectors. E_{proj} and E_{lab} correspond to energies in the projectile and laboratory frames, respectively. Energies of the Lyman line are taken from Ref. [38]. For $2s \rightarrow 1s$ we provide the energy of the center of the theoretical distribution of the $2E1$ decay mode [39].

	E_{proj}	$E_{\mathrm{lab}}(\Theta_L)$	Transmission T
$2p_{1/2} \rightarrow 1s$	3318.18	3831.36	$8.09 \times 10^{-7} (\pm 12\%)$
$2p_{3/2} \rightarrow 1s$	3322.99	3836.73	$8.09 \times 10^{-7} (\pm 12\%)$
$3p \rightarrow 1s$	3935.36	4543.78	$2.61 \times 10^{-6} (\pm 17\%)$
$4p \rightarrow 1s$	4150.19	4791.82	$2.63 \times 10^{-6} (\pm 17\%)$
$5p \rightarrow 1s$	4249.60	4906.60	$2.59 \times 10^{-6} (\pm 17\%)$
$2s \rightarrow 1s$	1660	1636	$4.43 \times 10^{-6} (\pm 4\%)$

($\pm 5\%$) μg/cm^2 (i.e., from 105 Å to 8000 Å) are used. Target thicknesses and purity are measured by 1–2 MeV α-particle Rutherford backscattering method, which has been performed before and after the GANIL irradiation. Only targets where impurities (mainly oxygen) contribute less than 3% to the total capture signal have been retained. The effective target thickness can also be varied by tilting the target with respect to the beam axis. This allows a fine scanning (i.e., overlapping measurements with different foils) and to extend the range of thickness up to 230 μg/cm^2 (11000 Å). We note that the total interaction (penetration) time of the beam with the thinnest foil is less than 9 a.u. or 200 attoseconds. This corresponds to an impulse electronic excitation on an ultrashort time scale comparable to shortest xuv pulses currently available [35]. Either CH_4 or N_2 have been used as gaseous targets and lead both to identical results in the ratio between different fine structure components as discussed in the last section.

To reach high precision in the measurements of Lyman intensities, we employ high-transmission high-resolution Bragg-crystal spectrometers specifically designed for this type of experiment. A resolution better than 5 eV is required to resolve the two fine-structure components $2p_j$ (see Table II, for Lyman energies) while keeping the detection efficiency as high as possible taking into account the low counting rates. Their principle of operation has been already described in detail in Ref. [36]. Briefly summarized here, high transmission is achieved by using a highly oriented pyrolytic graphite (HOPG) crystal with a mosaic spread of 0.4°, and a large (60×60 mm^2) home-made localization chamber. This position sensitive detector, working in the proportional regime, is filled with 1.15 atm of Ar(CH_4) and sealed by a thin aluminized Mylar window (12 μm of Mylar and 10 μg/cm^2 of Al). The spatial resolution reached was better than 500 μm. The two spectrometers are used in a vertical geometry to remove line broadening due to the Doppler effect and placed at an angle $\Theta_L = 30°$ on each side of the beam axis. For this geometry and angle, the recorded 4 keV line intensities are polarization-insensitive (the graphite crystal acting as a polarizer). Also, if the two arms of the spectrometers have equal length (equal target-to-crystal and crystal-to-detector distances), the effects associated with the mosaic spread vanish at first order. Under these conditions, the largest remaining contribution to the system resolution comes from the optical quality of the beam which has been considerably improved using a specific configuration of the GANIL facility; we make use of the first cyclotron (CSS1) combined together with the alpha spectrometer that allows, thanks also to the beam optics elements of the LISE beam line, to get high current intensity (up to 800 nA e) within a beam spot less than 1 mm of height and an almost horizontal parallel beam of a width around 6 mm. Finally, the spectrometer I, with two equal arms of 1630 mm length, was specifically designed to record the fine structure components of the $2p_j \rightarrow 1s$ transition and a resolution of ~2.5 eV at 3.8 keV was achieved [see Fig. 7(a)]. The spectrometer II, with two equal arms of 775 mm length, allows to obtain precisely either the $3p \rightarrow 1s$ transition [Fig. 7(b)] or higher members of the Lyman series from $4p$ to the end [Fig. 7(c)] with a resolution of ~6.5 eV or 8 eV, respectively. Under these conditions, an overall crystal spectrometer transmission T_{np} of $\sim 10^{-6}$ is attained (see Table II).

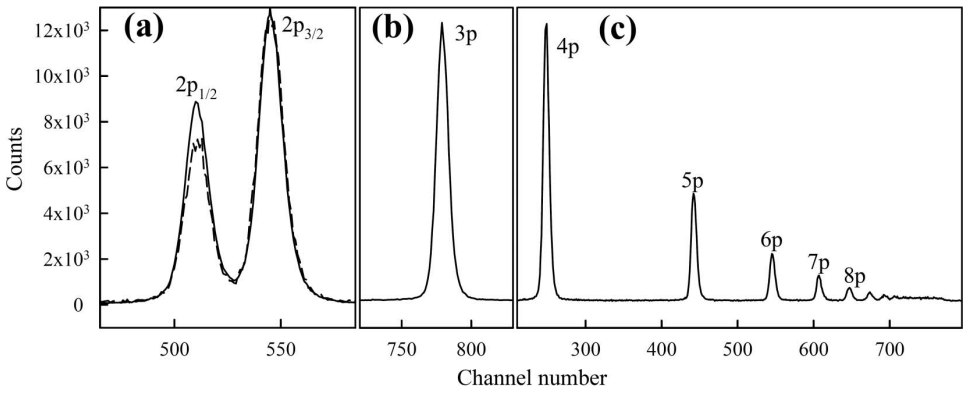

FIG. 7. Typical spectra recorded by the crystal spectrometers with a $d = 47.2$ μg/cm^2 (≈ 4300 a.u. ≈ 0.23 μm) carbon target thickness (solid lines): (a) observation of $2p_j \rightarrow 1s$ transitions (dashed line, spectrum obtained with a CH_4 gaseous target and normalized to the $2p_{3/2}$ component); (b) the $3p \rightarrow 1s$ transition (y axis $\times 3.5$); and (c) the higher members of the Lyman series (y axis $\times 12$).

To monitor these crystal spectrometers two Si(Li) detectors were placed at $\Theta_L=120°$ and $\Theta_L=150°$ with respect to the beam direction to record the complete series of Lyman $(np\rightarrow 1s)$ transitions emitted by the ion projectile. The energy resolution was 4% and 7% corresponding to linewidths of 125 eV at 3.02 keV ($\Theta_L=120°$) and 200 eV at 2.85 keV ($\Theta_L=150°$), respectively. Hence, we can clearly identify the Ar^{17+} $2p\rightarrow 1s$ and $3p\rightarrow 1s$ peaks.

The experimental population per incident ion $P_{np}^{\mathrm{exp}}(d)$ for a certain target thickness d is deduced from the recorded emission intensities, $I_{np\rightarrow 1s}(d)$, via the following equation:

$$P_{np}^{\mathrm{exp}}(d)=\frac{I_{np\rightarrow 1s}(d)}{B_{np\rightarrow 1s}N_{\mathrm{proj}}T_{np}}, \tag{4.1}$$

where $B_{np\rightarrow 1s}$ is the branching ratio and N_{proj} the number of ion projectiles. This population can be written as

$$P_{np}^{\mathrm{exp}}(d)=P_{np}(d)+P_{np}^{\mathrm{casc}}(d)+\gamma_{np}\int_0^d P_{np}(z)dz. \tag{4.2}$$

P_{np} stands for the population at the exit of the foil. Two aspects are to be considered: (i) after leaving the foil, higher excited states relax in a radiative cascade and thus contribute to the observed np populations through the term denoted by P_{np}^{casc} (for details see Ref. [37]); (ii) the emission during transport through the foil corresponds to the integrated population $P_{np}(d)$ weighted by the total decay rate γ_{np} of the observed transition. In the limit of very thin targets where the single collision condition is fulfilled, this third term is negligible and we can write

$$P_{np}^{\mathrm{exp}}(d)=P_{np}(d)+P_{np}^{\mathrm{casc}}(d). \tag{4.3}$$

The precision on the determination of the absolute np populations $P_{np}^{\mathrm{exp}}(d)$ leads to error bars not larger than 20% mainly due to the uncertainty on the global transmission T_{np} (see Table II). A comparison with the previous data (Ref. [6]) shows a discrepancy in the absolute magnitude of about a factor of 2 due to the fact that in Ref. [6] the absolute transmission was underestimated. Indeed, in Ref. [6], the detection system was specially designed to record the intensities of long-lifetime excited states and not the prompt intensities of the np states leading, in this case, to an underestimated absolute solid angle. Here, great care was taken on the evaluation of the transmission. Another pertinent quantity that can be also studied is the evolution of the relative Lyman intensities for which systematic experimental uncertainties cancel out. In particular those from fine-structure components like the ratio R_I,

$$R_I(d)=\frac{I_{2p_{1/2}\rightarrow 1s}(d)}{I_{2p_{3/2}\rightarrow 1s}(d)}, \tag{4.4}$$

where the error is only due to statistical uncertainties and Bremsstrahlung background. In the present paper, we will present only the values measured in the case of gaseous targets, which will be discussed and compared to the initial capture density matrix source term in a subsequent section. Experimentally, whatever the gas (CH_4 or N_2), we found a value of 0.54 ± 0.01 (2%).

Most of the populated exited states decay via single photon modes towards the ground state very fast, i.e., immediately after leaving the foil within a few 10^{-14} s for the np states. On the other hand, the $2s$ state has a lifetime of 3.5×10^{-9} seconds for Ar^{17+} and decays via two modes: a two-photon mode ($2E1$) and a single photon magnetic mode ($M1$) with branching ratio of 97% and 3%, respectively [38,39]. At a projectile velocity of $v_p=23$ a.u. (i.e., an energy of 13.6 MeV/amu), the lifetime translates into a propagation distance of $z_{2s}=173.6$ mm. Consequently, only a small window, Δa, around a given distance $z=a$ behind the target can be covered by a spectrometer placed at 90° with respect to the beam axis. We choose an observation position of $a=50$ mm, and a specific collimator of $\Delta a=2.25$ mm was designed to combine good enough detection efficiency (a few 10^{-6}, Table II) and spatial resolution that ensures enough precision in the determination of the $2_{s_{1/2}}$ population. Typical spectra are shown in Ref. [40]. The $2s$ state population is deduced from the recorded $2E1$ intensity, I_{2E1}, by the following relation:

$$P_{2s}^{\mathrm{exp}}(d)=\frac{I_{2E1}(d)}{2B_{2s\rightarrow 1s}^{2E1}N_{\mathrm{proj}}T_{2s}\displaystyle\int_{a-\Delta a}^{a+\Delta a}e^{-z/z_{2s}}dz}, \tag{4.5}$$

where $B_{2s\rightarrow 1s}^{2E1}=97\%$ denotes the branching ratio and T_{2s} the global transmission of the particular setup used. The uncertainty on $P_{2s}^{\mathrm{exp}}(d)$ is found around 15% for the full range of target thickness. The present experimental data on the evolution of the absolute $2s$ population as a function of carbon target thickness are fully consistent with our previous measurements that were acquired during a previous experiment dedicated to the production and transport of long-lifetime excited states alone [6,40]. The experimental observables we will discuss and compare with theoretical calculations are the np populations $P_{np}^{\mathrm{exp}}(d)$, the metastable $2s$ population $P_{2s}^{\mathrm{exp}}(d)$, and the $2p$ fine structure ratio for gaseous targets.

V. COMPARISON BETWEEN THEORY AND EXPERIMENT

In this section we present numerical results obtained by the QTMC simulation and compare them with the experimental data. We investigate different aspects of the time evolution of the reduced density matrix $\sigma_{\alpha\beta}(t)$ ranging from the ultrashort limit of single collision conditions to transport effects due to multiple scattering. The relative shell populations are considerably modified by transport (Fig. 8). Unless otherwise stated, we use the capture density matrix obtained by the LTDSE calculation for $n\leq 4$. For $n=4$ we use for the off-diagonal elements relative coherences calculated using the CDW approximation. In the single capture regime, or equivalently at short propagation lengths, capture into $n=2$ is dominant. The relative populations are directly proportional to the cross sections in Fig. 5 plus cascade contributions as indicated in Eq. (4.3). With increasing transport length excited states get either ionized by collisions or radiatively cascade to the ground state. Therefore the relative weight of $P(n=1)$ increases while all $P(n>1)$ get depleted during transport relative to P, the total occupation of Ar^{17+}. The

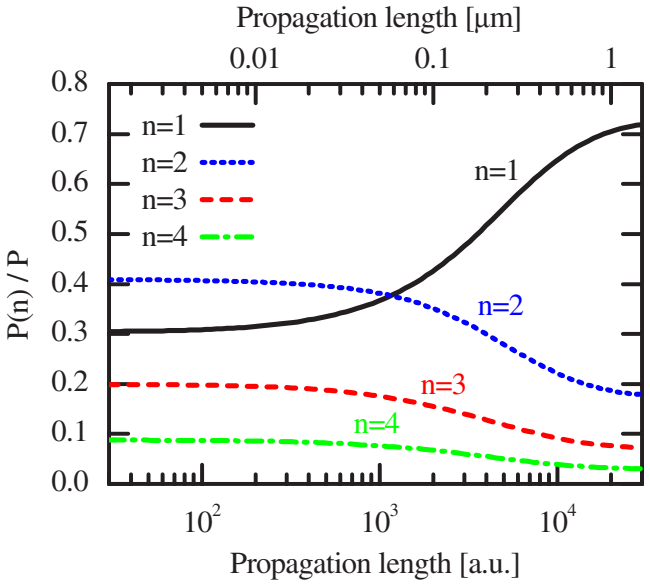

FIG. 8. (Color online) Evolution of relative n-shell populations of Ar^{17+} populated by electron capture as a function of propagation length through carbon foils. The simulated shell populations $P(n)$ are normalized to the overall charge state probability P of Ar^{17+}.

ratios between $P(n=2)$, $P(n=3)$, and $P(n=4)$ population fractions remain almost constant. The long time limit is characterized by three components: (i) feeding by capture, (ii) collisional excitation of the ground state, and (iii) collisional redistribution and ionization of excited states and intrashell mixing by the wake field. At the longest propagation length considered ($d=3\times10^4$ a.u.) an equilibrium seems to be established between these different processes.

By examining the relative populations of different states within each shell (Fig. 9) we can investigate transport effects in more detail. According to Fig. 4, capture cross sections are largest for p states and rapidly decrease for states with higher angular momentum. This general trend is reproduced by all approximations employed for the initial capture. On the other hand, transport tends to populate higher angular momentum states as is clearly seen in Fig. 9 at large propagation lengths. This is due to the interplay of two processes: collisions and mixing by the wake field. Collisions tend to drive the angular momentum of the bound electron to large $|m|$, where the quantization axis is aligned with the beam axis. The wake potential, by contrast, is responsible for l mixing while preserving m_l. The interplay of both processes makes states with all magnitudes and orientations of angular momentum rapidly accessible [6]. For the present collision system the consequence is that in the limit of long propagation lengths the relative intrashell probabilities are statistically distributed. In other words, the distribution within each shell is proportional to the number of available states $\sim 2l+1$. Overall, we observe a dramatic change of relative populations from the single-collision capture limit to equilibrium mixing, which is reached at propagation lengths of $d\approx2000$ a.u.

The dependence of experimental populations deduced from emitted photon intensities on the electron capture density matrix is shown in Fig. 10. Transport simulations using G^{CDW} and G^{LTDSE} agree with experimental data in the entire

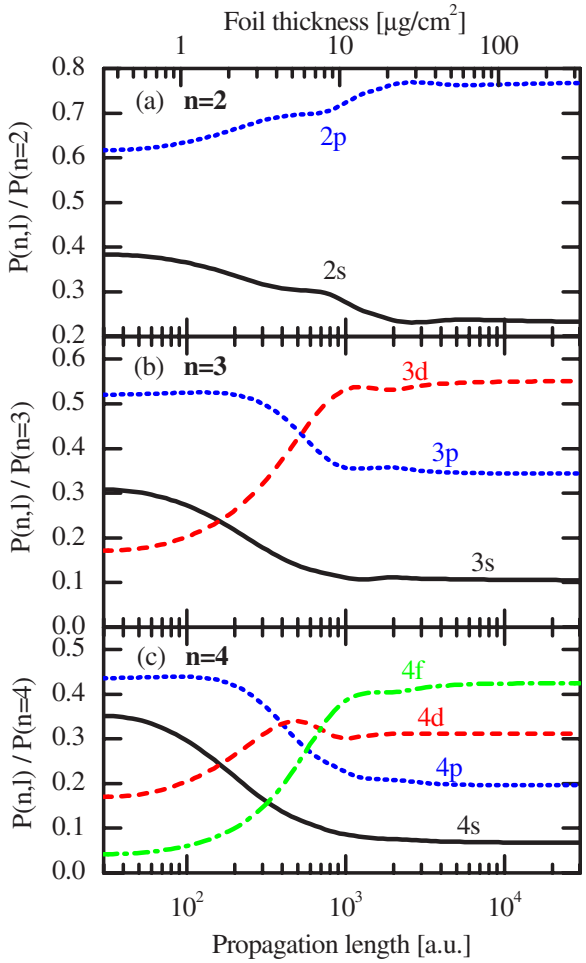

FIG. 9. (Color online) Evolution of relative populations of Ar^{17+} initially populated by electron capture as a function of propagation length through carbon. The simulated populations are presented as a function of n and l. The results are normalized to the overall probability in the corresponding shell: (a) $P(n=2,l)$; (b) $P(n=3,l)$; and (c) $P(n=4,l)$.

range of interaction times confirming the accuracy of capture cross sections in the single capture regime and of the description of the dynamical evolution. For thin foils the results reflect the single-collision capture cross sections. When looking closer we observe that G^{LTDSE} reproduce the measurements slightly better than those obtained by CDW for p states. This is due to the fact that cross sections for electron capture into p states obtained by the CDW approximation are smaller than those obtained by LTDSE. The resulting difference in photon intensities persists during transport.

Since CTMC cross sections for capture into p states are higher than those obtained with LTDSE, populations calculated using G^{CTMC} are larger than the present measurements. Results using G^{CTMC} are within the experimental resolution for the $2s$ intensity in the single collision regime but the discrepancy increases during transport as the $2s$ state mixes with other states. These conclusions contrast those found in Ref. [6] and are due to improvements in the calibration of the experimental data (the present intensities for p states are somewhat smaller than those reported in Ref. [6]).

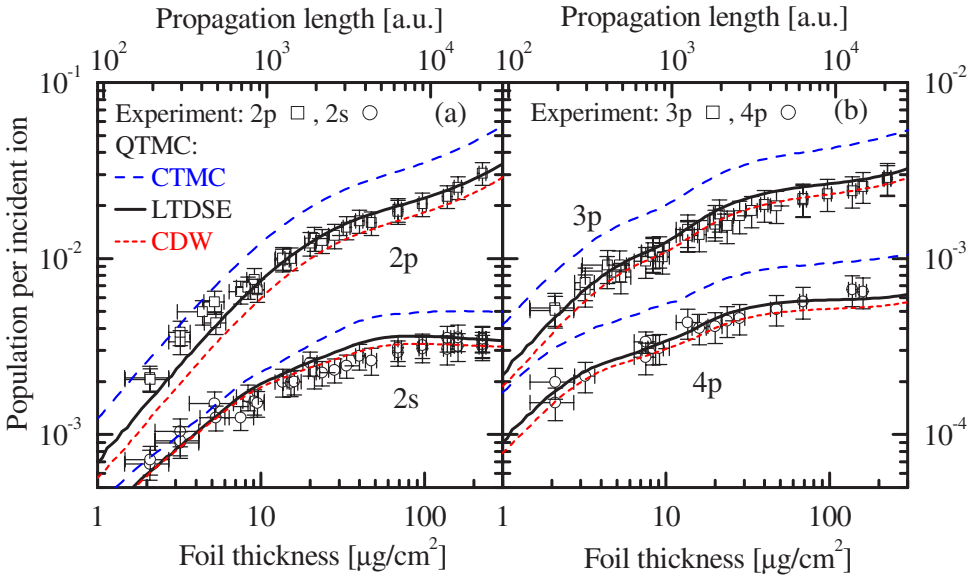

FIG. 10. (Color online) Absolute populations $P_{np,2s}(d)$ of excited Ar^{17+} ions as a function of foil thickness during transport through an amorphous carbon foil (v_p=23 a.u.) for (a) n=2 and (b) n=3,4. Symbols: experimental data; lines, results from full simulation within the QTMC method using different capture density matrices as input: solid lines, LTDSE; dotted lines, CDW; dashed lines, CTMC.

Alternatively to the present QTMC method, the Lindblad master equation can also be solved directly using a limited set of couplings. An example of such an approach is the master equation approach (MEA) [12,36] in which the collisional transition rates are calculated in plane-wave first Born approximation and the wake field is calculated following [41]. Figure 11 displays results from the MEA with the same electron capture density matrix used in our QTMC approach. The MEA results agree with the data for thin foils while it overestimates the populations for longer propagation lengths. These differences to the QTMC solution emerge in the mixing region starting at about 10 $\mu g/cm^2$ pointing to different treatments of the dynamics. Also shown for comparison in Fig. 11 are photon intensities obtained from our classical transport theory (CTT) to follow the time evolution of the active electron [6] and using an incoherent capture source calculated with CDW. The differences with respect to QTMC are not dramatic and the largest ones are observed for increasing foil thickness for the 2s, 3p, and 4p intensities. These differences are mainly due to the fact that the CTT simulations displayed in the figure neglect (i) coherences in the electron capture source and (ii) the radiative decay while ion is inside the solid. Overall, QTMC results describe the data more accurately than the other approaches and the

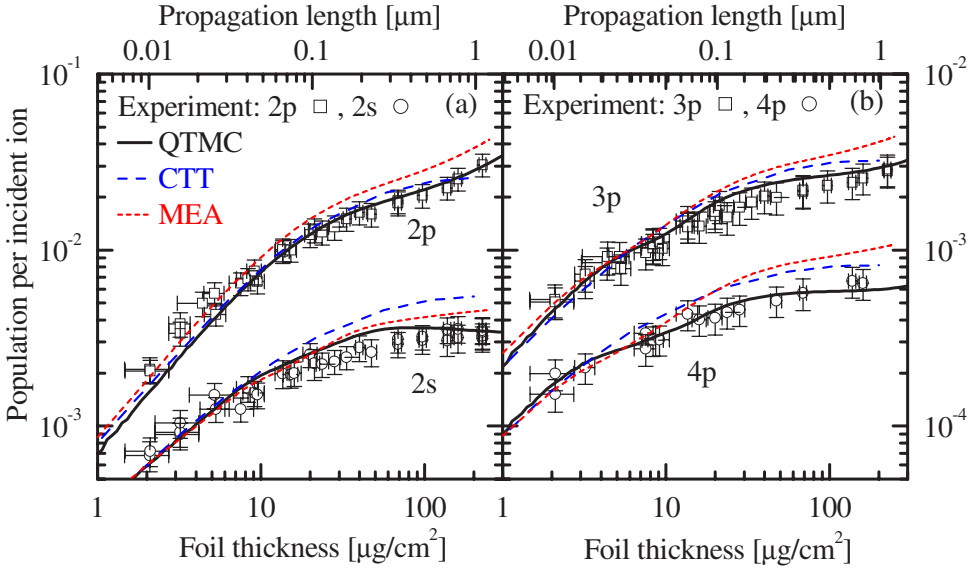

FIG. 11. (Color online) Absolute populations $P_{np,2s}(d)$ of excited Ar^{17+} ions as a function of foil thickness during transport through an amorphous carbon foil (v_p=23 a.u.) for (a) n=2 and (b) n=3,4. Symbols, experimental results; solid lines, QTMC results using LTDSE for capture; dashed lines, CTT calculation using CDW for capture; dotted lines, MEA calculation using LTDSE for capture into $n \leq 3$ and CDW for capture into $n > 3$.

LTDSE method provides the most accurate input for electron capture.

VI. SUMMARY AND OUTLOOK

We have presented a joint theoretical and experimental study of the production and transport of electronic states during the passage of Ar^{18+} ions through amorphous carbon foils. We have addressed two different aspects of the ion-solid interaction: (i) the production of excited states in electron capture and (ii) the modification of these states in transport through a solid.

We have performed accurate calculations of the electron capture density matrix as initial conditions for quantum transport by means of the solution of the time dependent Schrödinger equation on a lattice (LTDSE) and compared them with results obtained by the classical trajectory Monte Carlo (CTMC) method and by the continuum distorted wave (CDW) approximation. The agreement with measurements validates our nonrelativistic quantum mechanical calculations (CDW and LTDSE).

We have described the transport of electronic states through a solid by means of an open quantum system approach. We have developed an extension of the standard open quantum system approach to account for probability flux into the simulated system as well as out of the system. Along these lines we proposed an inhomogeneous Lindblad master equation and its solution by a quantum trajectory Monte Carlo method. This generalization enables us to incorporate ionization as well as electron capture. The overall good agreement between theory and experiment demonstrates the accuracy of the calculation and underlines the validity of the present approach. Overall, the present open quantum system approach and the new measurements have been found to be in much better agreement than previous comparisons [6].

There remains, however, one noteworthy discrepancy that appears already in the single collision regime and thus points to a deficiency of the diagonal elements $G(n,l,j)$ of the initial capture density matrix: the ratio between different fine structure components is, as long as the capture is treated to be spin independent, fixed by the transformation matrix between orbital angular momentum and fine structure states (nlj) (Clebsch-Gordan coefficients) as

$$G(n,l,j) = \frac{1}{2}\frac{2j+1}{2l+1}G(n,l). \tag{6.1}$$

Equation (6.1) predicts, for example, that $G(2p_{1/2})/G(2p_{3/2})=1/2$. This ratio is independent of the particular approximation of the capture density matrix. Experimentally, this ratio is found to be systematically enhanced by 10% to about $I_{2p_{1/2}\to 1s}/I_{2p_{3/2}\to 1s}=0.54\pm 0.01$. We surmise that this discrepancy is due to the onset of relativistic effects at $v_p=23$ a.u. $(v_p/c=0.17)$. Preliminary calculations employing the relativistic eikonal approximation (REA) [42–44] indicate that this ratio is indeed enhanced by relativistic effects, however the magnitude of the enhancement is insufficient to explain the experimental data in detail. As the region of validity of the REA lies at higher interaction potentials the partial agreement is inconclusive. This problem awaits further study by extending lattice-based solutions of electron capture using the Dirac equation or other relativistic approximations.

Finally we would like to point out that the Lindblad equation and its Monte Carlo solution can be used as a versatile tool adaptable to describe the coherent dynamics of a wide range of quantum systems that are strongly perturbed by their environment. The present formulation is expected to have applications beyond the field of ion-solid interactions. Examples include the coherent dynamics of electrons in quantum dots and quantum wells driven by THz pulses where electrons are continuously captured from and lost to the conduction band. The generalization presented here overcomes the restriction of the Lindblad master equation to unitary evolution making it a powerful framework for a large number of problems. Further extensions, in particular inclusion of contributions beyond the Markov approximation (i.e., memory effects) do not play a significant role in the present context but may be of importance in other systems and are deferred to further study.

ACKNOWLEDGMENTS

This work was supported by the FWF (Austria) special research project SFB016 "ADLIS," by the FWF projects P15025-N08 and P16871-N08 and by EU-projects HITRAP (HPRICT-2001-50036) and ITS-LEIF (HPRI-CT-2005-026015). This work was also supported by the U.S. DOE Office of Fusion Energy Sciences, including a SciDAC grant administered through Auburn University, and from the Office of Basic Energy Sciences, to Oak Ridge National Laboratory which is managed by UT-Battelle, LLC under Contract No. DE-AC05-00OR22725. The authors would like to acknowledge helpful discussions with Jörg Eichler, Akira Ichihara, and Florian Aigner. The authors address specific thanks to the staff of CIRIL and GANIL for providing us with outstanding technical assistance and exceptional high-quality beams. The authors are also grateful to Lamri Adoui, Amine Cassimi, Brigitte Ban d'Etat, Benoit Gervais, Céline Lauhlet, Medhi Tarisien, and Jean Marc Ramillon for their participation in the data acquisition.

[1] R. Dum, P. Zoller, and H. Ritsch, Phys. Rev. A **45**, 4879 (1992).
[2] K. Mølmer, Y. Castin, and J. Dalibard, J. Opt. Soc. Am. B **10**, 524 (1993).
[3] T. Minami, C. O. Reinhold, and J. Burgdörfer, Phys. Rev. A **67**, 022902 (2003).
[4] M. Seliger, C. O. Reinhold, T. Minami, and J. Burgdörfer, Phys. Rev. A **71**, 062901 (2005).
[5] M. Seliger, Ph.D. thesis, Vienna University of Technology, 2005.
[6] C. O. Reinhold, D. G. Arbó, J. Burgdörfer, B. Gervais, E. Lamour, D. Vernhet, and J.-P. Rozet, J. Phys. B **33**, L111 (2000).
[7] T. Minami, C. O. Reinhold, D. R. Schultz, and M. S. Pindzola, J. Phys. B **37**, 4025 (2004).
[8] J. Dalibard, Y. Castin, and K. Mølmer, Phys. Rev. Lett. **68**, 580 (1992).
[9] H. J. Carmichael, Phys. Rev. Lett. **70**, 2273 (1993).
[10] G. Lindblad, Commun. Math. Phys. **48**, 119 (1976).
[11] G. Lindblad, Rep. Math. Phys. **10**, 393 (1976).
[12] D. Vernhet, C. Fourment, E. Lamour, J.-P. Rozet, B. Gervais, L. J. Dubé, F. Martin, T. Minami, C. O. Reinhold, M. Seliger, and J. Burgdörfer, Phys. Scr., T **T92**, 233 (2001).
[13] C. W. Gardiner and P. Zoller, *Quantum Noise* (Springer, Berlin, 1999).
[14] P. M. Echenique, R. H. Ritchie, and W. Brandt, Phys. Rev. B **20**, 2567 (1979).
[15] P. M. Echenique, W. Brandt, and R. H. Ritchie, Phys. Rev. B **33**, 43 (1986).
[16] J. H. McGuire and L. Weaver, Phys. Rev. A **16**, 41 (1977).
[17] B. Gervais, C. O. Reinhold, and J. Burgdörfer, Phys. Rev. A **53**, 3189 (1996).
[18] J. Burgdörfer and J. Gibbons, Phys. Rev. A **42**, 1206 (1990).
[19] J. Kemmler, J. Burgdörfer, and C. O. Reinhold, Phys. Rev. A **44**, 2993 (1991).
[20] I. M. Cheshire, Proc. Phys. Soc. London **84**, 89 (1964).
[21] D. S. F. Crothers and J. F. McCann, J. Phys. B **17**, L177 (1984).
[22] D. Belkic, R. Gayet, and A. Salin, Comput. Phys. Commun. **32**, 385 (1984).
[23] J. Burgdörfer and K. Taulbjerg, Phys. Rev. A **33**, 2959 (1986).
[24] R. Abrines and I. C. Percival, Proc. Phys. Soc. London **88**, 861 (1966); **88**, 873 (1966).
[25] R. E. Olson and A. Salop, Phys. Rev. A **16**, 531 (1977).
[26] R. E. Olson, Phys. Rev. A **24**, 1726 (1981).
[27] C. O. Reinhold and C. A. Falcon, Phys. Rev. A **33**, 3859 (1987).
[28] D. R. Schultz, P. C. Stancil, and M. J. Rakovic, J. Phys. B **34**, 2739 (2001).
[29] A. Kolakowska, M. S. Pindzola, F. Robicheaux, D. R. Schultz, and J. C. Wells, Phys. Rev. A **58**, 2872 (1998).
[30] D. R. Schultz, M. R. Strayer, and J. C. Wells, Phys. Rev. Lett. **82**, 3976 (1999).
[31] A. Kolakowska, M. S. Pindzola, and D. R. Schultz, Phys. Rev. A **59**, 3588 (1999).
[32] R. H. Garvey, C. H. Jackman, and A. E. S. Green, Phys. Rev. A **12**, 1144 (1975).
[33] D. R. Schultz and C. O. Reinhold, Comput. Phys. Commun. **114**, 342 (1998).
[34] J. Burgdörfer, Phys. Rev. A **24**, 1756 (1981).
[35] R. Kienberger *et al.*, Nature (London) **427**, 817 (2004).
[36] D. Vernhet, J.-P. Rozet, I. Bailly-Despiney, C. Stephan, A. Cassimi, J-P. Grandin, and L. J. Dubé, J. Phys. B **31**, 117 (1998).
[37] T. Minami, C. O. Reinhold, M. Seliger, J. Burgdörfer, C. Fourment, E. Lamour, J.-P. Rozet, D. Vernhet, and B. Gervais, Phys. Rev. A **65**, 032901 (2002).
[38] P. Indelicato (*private communication*).
[39] S. P. Goldman and G. W. F. Drake, Phys. Rev. A **24**, 183 (1981).
[40] E. Lamour, B. Gervais, J.-P. Rozet, and D. Vernhet, Phys. Rev. A **73**, 042715 (2006).
[41] J.-P. Rozet, D. Vernhet, I. Bailly-Despiney, C. Fourment, and L. J. Dubé, J. Phys. B **32**, 4677 (1999).
[42] J. Eichler, Phys. Rev. A **32**, 112 (1990).
[43] J. Eichler, Phys. Rep. **193**, 165 (1990).
[44] J. Eichler and A. Ichihara (private communication).